Journal of Catalysis 367 (2018) 306–314

Contents lists available at ScienceDirect

Journal of Catalysis

journal homepage: www.elsevier.com/locate/jcat

Insight into the deactivation mode of methanol-to-olefins conversion over SAPO-34: Coke, diffusion, and acidic site accessibility

Shushu Gao [a,b], Shutao Xu [a,*], Yingxu Wei [a,*], Qinglong Qiao [c], Zhaochao Xu [c], Xinqiang Wu [a,b], Mozhi Zhang [a], Yanli He [a], Shuliang Xu [a], Zhongmin Liu [a,d,*]

[a] National Engineering Laboratory for Methanol to Olefins, Dalian National Laboratory for Clean Energy, iChEM (Collaborative Innovation Center of Chemistry for Energy Materials), Dalian Institute of Chemical Physics, Chinese Academy of Sciences, Dalian 116023, People's Republic of China
[b] University of Chinese Academy of Sciences, Beijing 100049, People's Republic of China
[c] Key Laboratory of Separation Science for Analytical Chemistry, Dalian Institute of Chemical Physics, Chinese Academy of Sciences, Dalian 116023, People's Republic of China
[d] State Key Laboratory of Catalysis, Dalian Institute of Chemical Physics, Chinese Academy of Sciences, Dalian 116023, People's Republic of China

ARTICLE INFO

Article history:
Received 26 March 2018
Revised 14 August 2018
Accepted 9 September 2018

Keywords:
Methanol-to-olefins conversion
SAPO-34
Coke
Intracrystalline diffusion
Acidity

ABSTRACT

The whole reaction course of methanol-to-olefins (MTO) conversion over SAPO-34 catalyst with crystal size 7–10 μm has been investigated by multiple spectroscopic techniques. The reaction and deactivation of methanol conversion are closely correlated to the amount, size, and location of coke formed in the CHA nanocages. A nonuniform spatial distribution of these coke species in the individual SAPO-34 crystals is revealed by a combination of hyperpolarized (HP) ^{129}Xe NMR and confocal fluorescence microscopy (CFM) techniques. Combined with acidic properties and diffusion performance, the bulky coke species formed at the shell layer of the crystals led to an increase of intracrystalline diffusion resistance and a decrease in accessible acidic sites in the deactivated catalyst. The overall catalyst deactivation mode of the MTO reaction is presented in terms of coke formation and location, mass transport variation, and accessibility of Brønsted acid sites in the SAPO-34 catalyst.

1. Introduction

The production of light olefins (ethene and propene) via a non-petroleum route of methanol-to-olefins (MTO) reaction over solid acid catalysts has attracted widespread attention from the academy and industry [1–3]. The MTO reaction is catalyzed by shape-selective zeolites with well-defined micropores and catalytical active sites [2,4–7]. The SAPO-34 molecular sieve with chabazite (CHA) topology and moderate acidity is the optimum catalyst for the MTO process. The spacious cavities in CHA-type SAPO catalysts, interconnected by narrow eight-membered ring windows, favor the formation and accommodation of large aromatic species, which obstruct the diffusion of higher hydrocarbon products, leading to extremely high selectivity toward light olefins. Over the past four decades, extensive efforts have been devoted to the MTO reaction mechanism and there is a consensus that the hydrocarbon pool mechanism, proposed by Dahl and Kolboe, is responsible for the formation of light olefins during the steady-state reaction stage [8–12]. Previous studies on the identification and the role of hydrocarbon pool species have concluded that methylbenzenes and their protonated counterparts form in the cavities as catalytic active intermediates over SAPO-34 [10,11]. However, these intermediates could grow into heavier carbonaceous deposits on the acidic sites of catalysts, termed "coke," which eventually lead to quick catalyst deactivation in the MTO reaction [12–14]. Catalyst deactivation by coke formation depresses the raw material utilization efficiency in the industrial application of the MTO process.

Many efforts have been made to illustrate catalyst deactivation in terms of the nature, role, and spatial distribution of coke formed on SAPO-34 catalysts [12,15–18]. Catalyst deactivation pathways vary with catalyst topology and reaction temperature [13,17,19,20]. On one hand, the location of coke depends on the zeolite topology. SAPO-34 shows pronounced formation of coke deposits inside the cavities of crystals in comparison with ZSM-5 [12,21]. On the other hand, the chemical composition of coke varies with reaction temperature. At lower temperatures, less than 623 K, rapid deactivation is closely related to the generation of

* Corresponding authors at: National Engineering Laboratory for Methanol to Olefins, Dalian National Laboratory for Clean Energy, iChEM (Collaborative Innovation Center of Chemistry for Energy Materials), Dalian Institute of Chemical Physics, Chinese Academy of Sciences, Dalian 116023, People's Republic of China.
E-mail addresses: xushutao@dicp.ac.cn (S. Xu), weiyx@dicp.ac.cn (Y. Wei), liuzm@dicp.ac.cn (Z. Liu).

https://doi.org/10.1016/j.jcat.2018.09.010
0021-9517/

adamantane hydrocarbons, which are inactive for methanol conversion as confined organics inside the cavities of SAPO-34 catalysts [17,18]. At higher temperatures, more than 673 K, methanol conversion tends to form polymethylbenzenes, which behave not only as important intermediates for olefin production, but also as precursors for forming polyaromatics, such as methylnaphthalenes, phenanthrene, and pyrene, as coke species [12,16]. Also, methylbenzenes and methylnaphthalenes are capable of acting as important intermediates during the steady-state reaction period [10,11,22,23]. Additionally, a lower coking rate is presented in the temperature range of 673–723 K than at higher (773 K) or lower (573 K) temperature and leads to mild catalyst deactivation over SAPO-34 during the MTO reaction [18]. The formation of these bulky carbonaceous deposits as coke species within the cavities of SAPO-34 is known to depress the conversion of methanol and limit mass transport by blocking pore entrances in the course of catalytic processes [16]. Mass transport in porous catalysts could affect the overall reaction rate or even product selectivity [24–27]. Small SAPO-34 crystals have been reported to show a longer lifetime and a lower coke rate due to reduced diffusion limitation in the MTO process [24–26,28,29]. In addition, the acidic properties of catalysts strongly influence the catalytic performance [30–32] and the accessibility of acidic sites of the catalyst is closely associated with coke deposition. The number of accessible Brønsted acid sites of the SAPO-34 catalyst was greatly reduced due to coke formation [26,33–35].

Catalyst deactivation is considered a crucial problem to be resolved to improve catalytic performance. The formation and evolution of retained organics, including the active intermediates and coke species, induce the process of methanol reaction and catalyst deactivation, and in this dynamic process, coke formation also influences olefin product generation. The whole recognition of the spatial distribution of coke species and the effect of their accommodation on mass transport and the acidic properties of the catalyst is of great importance for further optimizing MTO processes and catalysts. Therefore, a comprehensive investigation of catalyst deactivation is highly desirable.

In the present work, methanol conversion was performed over a SAPO-34 catalyst with crystal size 7–10 μm under mild reaction conditions at 673 K for further deactivation analysis. The dynamic processes of reaction and catalyst deactivation were studied by multiple techniques such as gas chromatography–mass spectrometry (GC–MS), thermogravimetric analysis (TGA), hyperpolarized (HP) ^{129}Xe NMR, confocal fluorescence microscopy (CFM), ultraviolet–visible spectroscopy (UV–vis), diffuse reflectance infrared Fourier transform spectroscopy (DRIFTS), and ^{1}H pulsed field gradient (PFG) nuclear magnetic resonance (NMR). Confocal fluorescence microscopy has been successfully applied to monitor coke formation and distribution on individual crystals during the MTO reaction, and the emergence of this technique has contributed notably to the understanding of catalyst deactivation [15,36,37]. ^{129}Xe NMR spectroscopy is a technique with particular use in probing the internal pore structure and different local chemical environments of porous materials due to the high sensitivity of the large electron cloud of xenon [38–40]. After hyperpolarization by optical pumping, its sensitivity is be enhanced by 4–5 orders of magnitude, which allows the highly sensitive detection of very small numbers of adsorption sites in sample and the reduction of acquisition time [40,41]. In addition, pulsed field gradient (PFG) NMR, a very effective technique for the measurement of guest molecular diffusion in confined nanoporous materials, has been used to study the self-diffusion coefficients of molecules in SAPO-34 catalysts [16,42–44]. Based on these techniques, we have clarified how coke formation and distribution affect methanol reaction and product generation by modifying the acidity and mass transport of SAPO-34 catalysts in the MTO reaction.

2. Experimental

2.1. Catalyst synthesis

SAPO-34 was hydrothermally synthesized using the triethylamine (NEt_3) as an organic template. Pseudoboehmite (67.5 wt%), phosphoric acid (85 wt%), and silica sol (30 wt%) were used as aluminum, phosphorus, and silicon sources, respectively. The initial gel ratio of SAPO-34 was 1.0 Al_2O_3:1.0 P_2O_5:0.4 SiO_2:3 NEt_3:80 H_2O. Typically, the mixture of pseudoboehmite, phosphoric acid, silica sol, and deionized water was stirred for 1 h to form a homogeneous aqueous solution and then triethylamine was added into the aqueous solution. The resulting gel was transferred into a stainless steel autoclave and crystallized at 473 K for 15 h. The solid product was washed with deionized water and dried at 393 K for 12 h. The catalyst for the MTO reaction was calcined at 873 K for 4 h to remove the template.

2.2. Catalyst characterization

The powder X-ray diffraction (XRD) pattern of the calcined SAPO-34 catalyst was recorded on a PANalytical X'Pert PRO X-ray diffractometer with CuKα radiation (λ = 1.5418 Å) to determine the crystallinity and purity of SAPO-34. The morphology of SAPO-34 crystals was obtained using a Hitachi SU8020 field emission scanning electron microscope. The chemical composition of the synthesized SAPO-34 molecular sieve was determined with a Philips Magix-601 X-ray fluorescence (XRF) spectrometer. X-ray photoelectron spectroscopy (XPS) was performed on a Thermo ESCALAB 250Xi using a monochromatic Al*K*α X-ray source (1486.6 eV, 15 kV, 10.8 mA). The surface atomic ratio was determined from the peak areas of Si2*p*, Al2*p*, and P2*p*, respectively.

Nitrogen adsorption–desorption was employed to determine the BET surface area and micropore volume of fresh and spent catalysts at 77 K (Micromeritics ASAP 2020). Fresh and spent catalysts were pretreated from 298 to 673 K and 473 K under vacuum, respectively.

2.3. Catalytic test

A MTO reaction was performed over SAPO-34 in a fixed-bed quartz reactor under atmospheric pressure. Catalyst particles (20–40 mesh) of 500 mg were loaded into the middle of the reactor and supported by quartz wool. The ratio of the height of the catalyst bed to the diameter of the reaction tube was 0.33. The catalyst was activated at 773 K for 1 h in a flow of helium gas prior to the reaction test. Then the temperature of the reactor was adjusted to 673 K for the methanol reaction. Methanol was fed by passing carrier gas through a saturation evaporator containing methanol at 32.5 °C, which gave a weight hourly space velocity (WHSV) of 4.0 h^{-1} and a He/methanol ratio of 3.1. A high gas flow rate (83 mL/min) of carrier gas and a thin catalyst bed (0.5 cm) in a reactor with large diameter (ca. 1.5 cm) used in the MTO reaction ensured the uniformity of catalyst deactivation along the catalyst bed for further catalyst characterization. The products were analyzed quantitatively using an online gas chromatograph (Agilent GC 7890A) equipped with an FID detector and an HP-PLOT Q capillary column. The reactions were performed under the same reaction condition and stopped at time on stream of 5, 10, 18, 49, and 96 min. After quenching with liquid nitrogen to stop the reaction, the spent catalyst particles taken from the whole catalyst bed were mixed and used for coke analysis, acidity, and diffusion measurements.

2.4. Coke amount, identification, and location

The coke amount of spent SAPO-34 catalysts after reaction was analyzed by thermogravimetric analysis (TGA) on a TA SDTQ600. The catalysts were heated from 298 to 1073 K at 10 K/min under an air flow of 100 mL/min. The chemical composition of coke species trapped in SAPO-34 was determined based on an approach described in the literature [33]. Spent catalysts (50 mg) were dissolved in a 20% HF solution; then the organic phase were extracted using CH_2Cl_2 solvent with internal standard C_2Cl_6 and analyzed by GC–MS (Agilent 7890/MSD).

The spatial distribution of coke species deposited on SAPO-34 catalysts with various reaction times was studied by combining HP ^{129}Xe NMR with confocal fluorescence microscopy. The HP ^{129}Xe NMR experiments were performed on a Varian Infinity-plus 400 spectrometer at the resonance frequency of 110.6 MHz. Prior to NMR tests, the fresh and spent samples were dehydrated under high vacuum for at least 12 h at 673 and 473 K, respectively. Continuous-flow hyperpolarized ^{129}Xe gas (a 1% Xe–1% N_2–98% He mixture) was obtained in an optical pumping cell with a laser in the experiments as depicted in the literature [38,40]. In the NMR measurement, a constant flow of gas mixture was delivered directly into the NMR tube at a rate of 150 mL/min. For each experiment, the same amount of catalyst particles (20–40 mesh) was loaded into the middle of the NMR tube and supported by quartz wool (Scheme S1 in the Supplementary Material). Temperature-dependent HP ^{129}Xe NMR spectra were obtained at 193, 233, and 293 K. Typically, one pulse sequence with a recycle delay of 2 s and 64 scans was used. Ultraviolet–visible (UV–vis) spectra of spent catalysts were recorded on a VARIAN Cary-5000 UV–Vis–NIR spectrophotometer equipped with an integration sphere in the range of 200–800 nm. For each experiment, the same amount of catalyst and the same test conditions were used. The fluorescence tests were conducted on an IX81 microscope (Olympus, Japan) coupled with an EMCCD camera (DU-897U-CS0-#BV, Andor, UK). The excitation wavelength was set to 700 nm, and emission in the range 760–840 nm was collected.

2.5. Pulsed field gradient NMR

The intracrystalline diffusion coefficients of molecules in fresh and spent catalysts were studied with ^{1}H PFG NMR experiments, which were carried out on a Bruker Avance III 600 spectrometer equipped with a Bruker diff50 diffusion probe and a maximum magnetic field gradient strength of 1800 G/cm in the z-direction. Considering the narrow eight-ring windows (3.8 × 3.8 Å) of the CHA topology, methane and ethene with small kinetic diameters of ca. 3.8 and 3.9 Å, respectively, were chosen for diffusion studies in ^{1}H PFG NMR [45]. The basic principle of PFG NMR is reported in detail elsewhere [42,46]. To avoid the effects of internal magnetic field gradients in the porous materials, a stimulated echo sequence with bipolar-gradient (13-interval sequence, PGSTEBP) was applied in all our experiments [47]. The spin–echo attenuation $I(g)/I(0)$ could be obtained by linearly increasing a series of gradient strength g in 16 steps, while the gradient duration δ and the diffusion time Δ were kept constant. Self-diffusion coefficients of adsorbed molecules can be obtained according to the Stejskal–Tanner equation,

$$I(g) = I(0)\exp\left[-(\gamma\delta g)^2 D\left(\Delta - \frac{\delta}{3}\right)\right], \quad (1)$$

where $I(0)$ and $I(g)$ are the signal amplitude using $g = 0$ and variable g, respectively, γ is the gyromagnetic ratio, δ is the effective gradient pulse duration, g is gradient strength, Δ is the diffusion time, and D is the self-diffusion coefficient. Under these conditions, the background signals of the diffusion probe and hydrocarbon species trapped in SAPO-34 were completely excluded due to their immobility. Temperature-dependent experiments were performed at 298, 308, 318, and 328 K to obtain the apparent diffusion activation energies, E_a.

Prior to ^{1}H PFG NMR tests, approximately 300 mg of catalysts was pretreated at 673 K for fresh and 473 K for spent catalysts under vacuum to completely remove adsorbed water in pore space. Subsequently, the samples were transferred into 5 mm NMR tubes in a N_2 glove box. Then the required adsorbate was introduced quantitatively into the NMR tube on a homemade uptake apparatus, and the tubes were sealed off. All data were acquired under equilibrium conditions. The loadings of adsorbed molecules are calculated according to the ideal gas equation.

2.6. Diffuse reflectance infrared Fourier transform spectroscopy

The Brønsted acidity of SAPO-34 catalysts with different reaction times was studied by DRIFTS on a Bruker Vextex70 spectroscope equipped with a MCT detector. For each experiment, the same amount of catalyst and the same test conditions were used. Prior to characterization, fresh and spent catalysts were heated at 723 and 473 K respectively for 3 h in the diffuse reflectance infrared chamber with a ZnSe window under helium to remove adsorbed water; then the DRIFT spectra were recorded by collecting 16 scans at resolution 4 cm^{-1}.

3. Results and discussion

3.1. Catalytic performance of methanol-to-olefins reaction over SAPO-34

The catalytic performance of methanol conversion over SAPO-34 with a crystal size of 7–10 μm (Fig. S2) at 673 K is presented in Fig. 1. Almost 100% methanol conversion over the SAPO-34 catalyst at the beginning of the reaction (0–18 min) indicated a stage of complete conversion of methanol in which the reactant passed through the whole catalyst bed. After this efficient reaction period, the decline of methanol conversion from 99.8% to 56% corresponds to obvious penetration of the reactant, which cannot be completely converted over the deactivated catalyst bed. After reaction for 96 min, most of the catalyst particles were seriously deactivated and methanol conversion was lower than 20%. Typically, ethene, propene, and higher olefins were produced as the main products,

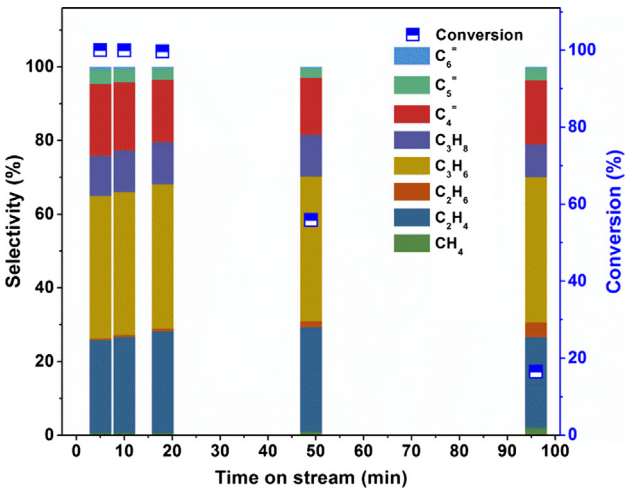

Fig. 1. Methanol conversion and product selectivity over SAPO-34 during the MTO reaction at 673 K.

and light alkanes, such as methane, ethane, and propane, are also generated. Among all the products, propene exhibited the highest yield among the gaseous products.

3.2. Evolution of the confined organic species over SAPO-34

3.2.1. The amount and chemical composition of coke species trapped inside catalysts

The amounts of coke formed on SAPO-34 catalyst after methanol reaction for various reaction times were quantified by TGA experiments. As shown in Fig. 2, initial reaction with complete methanol conversion for the beginning 5 min generated only a small amount of coke (coke amount 2.5 wt%). After reaction for 18 min, a significant enhancement of coke deposition occurred and the coke amount attained to 8.1 wt%; at the same time, a slight decrease was observed in methanol conversion. Further prolonging the reaction time to 49 min gave rise to coke growth in the catalyst and a decrease in methanol conversion. After reaction for 96 min, the catalyst was severely deactivated and the coke amount attained 15.8 wt%. These results clearly show that the decrease in the conversion rate becomes remarkable when the coke amount is more than 8.1 wt%; however, it is almost not affected by catalysts with small coke amounts.

A detailed study indicated that the coke species (Fig. S3) and their proportions (Fig. 2) in SAPO-34 catalyst vary with reaction time. The aromatic compounds are the main components of coke species retained on the catalysts. At 5 min, methylbenzenes (89%) were more predominantly formed on the catalyst than other organic components, in particular tetramethylbenzene, and a small amount of methylnaphthalenes (11%) also formed simultaneously (Fig. 2). It has been reported that methylbenzenes and methylnaphthalenes can act as hydrocarbon pool species and the latter has lower activity in SAPO-34 [23]. After reaction for 10 min, phenanthrene and pyrene were also detected at very low intensity. Furthermore, the proportions of bicyclic aromatics (methylnaphthalenes) and polycyclic aromatics (phenanthrene and pyrene) continued to increase with increased coke amount, especially methylnaphthalene hydrocarbons. The proportion of retained hydrocarbons shifted from 65% monocyclic, 34% bicyclic, and 1% polycyclic arenes after 18 min on stream to 35% monocyclic, 60% bicyclic, and 5% polycyclic arenes after 96 min on stream. Combining the coke composition with the coke amount, it could be concluded that the formation and accumulation of more condensed aromatics are responsible for the increased coke amount in catalysts with TOS and the reduction of MTO activity.

3.2.2. Spatial distribution of coke species trapped inside catalysts

Fig. 3 displays the relationship between textural properties (micropore volume and BET surface area) of catalysts and coke amount with the aid of N_2 adsorption–desorption measurements. Obviously, the variation of surface area and micropore volume showed the same trend with increasing coke amount. From 0 to 10 min, although the coke amount increased from 0 to 7.4 wt%, which is nearly half of the total coke increment during the whole reaction, the loss of surface area or micropore volume was only 12%, and high activity of the catalyst was retained during this reaction period. During this period, the formation of methylbenzenes and methylnaphthalenes, which were regarded as active intermediates, may slightly affect the intracrystalline mass transport and a large number of cages of crystal were still accessible for reactants. A sharp reduction in micropore volume and BET surface area of catalysts was observed at reaction times from 10 to 18 min, in which the catalyst went through a very slight increase in coke amount (from 7.4 to 8.1 wt%), indicating that very small incremental formation of organics leads to enhanced pore blockage during this short period. This change in textural properties could be related not only to the coke amount but also to the spatial distribution of coke species. For deactivated catalyst at 49 min, the micropore volume and BET surface area of the catalyst represent approximately 10% of the total micropore volume and BET surface area, respectively. This indicates that the accessible cages, which can be detected with nitrogen adsorption–desorption measurements, are greatly reduced by coke formation and accumulation. Therefore, coke formation and distribution on the catalyst strongly affect its porosity.

To obtain detailed insight into the coke distribution at the microscopic level, the temperature-variation HP ^{129}Xe NMR approach was followed to probe the heterogeneity of the porosity in the SAPO-34 catalysts with coke deposition during the MTO reaction. ^{129}Xe NMR spectroscopy proved to be a valuable tool for probing the internal channels or external surfaces of coked zeolites [48]. As shown in Fig. 4, the NMR peak at around 0 ppm represents xenon in the gaseous phase. The broad peak at higher chemical shift corresponds to adsorbed xenon in CHA nanocages of SAPO-34. When temperature decreased from 293 to 193 K, the chemical shift of adsorbed xenon increased with lower temperature and its peak width broadened, resulting from strong Xe–Xe

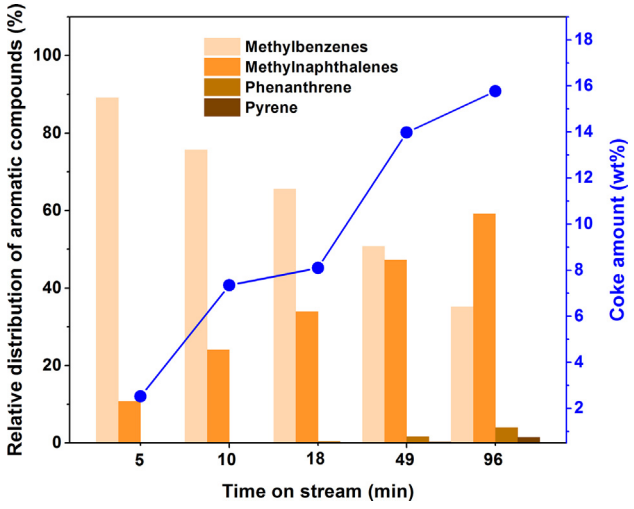

Fig. 2. Coke amounts of the spent SAPO-34 catalysts and the relative distribution of coke components of methylbenzenes, methylnaphthalenes, phenanthrene, and pyrene after reaction for different times.

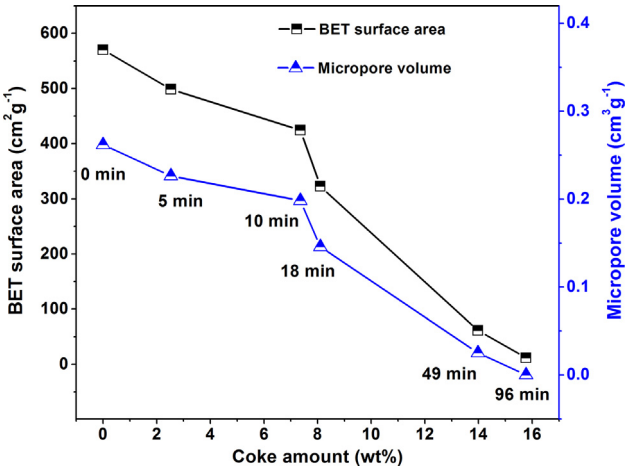

Fig. 3. The micropore volume and BET surface area of SAPO-34 catalysts as functions of coke amount.

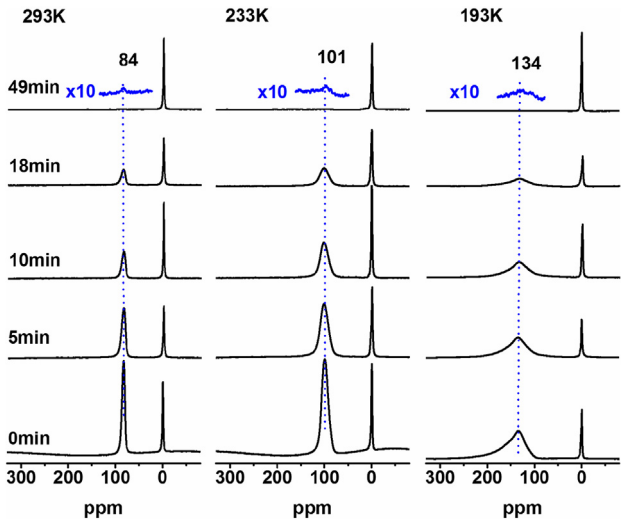

Fig. 4. Temperature-dependent HP ^{129}Xe NMR spectra of xenon adsorbed in fresh and spent SAPO-34 catalysts after MTO reaction at 673 K for various reaction times.

interaction [38,39]. The chemical shifts of xenon adsorbed in CHA nanocages of spent catalysts remain unchanged compared to those for fresh catalysts at the same temperature, and the intensities of these signals decreased obviously after reaction for a longer time. Thus the signal of adsorbed Xe does not come from coke-containing cages but from empty cages. This reveals that the distribution of coke is not uniform and some CHA cages in the crystal remain unoccupied during the reaction. As shown in Fig. S4, the variation of the relative intensity of adsorbed Xe at 293 K with the coke amount in SAPO-34 catalysts does not follow a linear relationship. Especially for the catalysts at 10 and 18 min, the coke amount only increased from 7.4 to 8.1 wt%; however, the relative intensity of the adsorbed Xe signal decreased fastest. This implies that coke formation during this period will greatly affect the adsorption performance of the catalyst, which leads to a sharp reduction in the accessibility of CHA nanocages. Based on TGA, GC–MS, and N_2 adsorption–desorption results, it is reasonable to speculate that the formation and accumulation of coke species in the cavities in the outer layer of the crystal induce a rapid decrease in the intensity of adsorbed xenon from 10 to 18 min and prevent xenon from entering the internal cavities. It is worth noting that the peak of adsorbed Xe was almost invisible at a reaction time of 49 min, indicating that the path of mass transport of xenon was severely obstructed by the coke formation. The cavities in the core of the crystal cannot be probed by xenon atoms in the deactivated catalyst after reaction for 49 min.

To further verify the aforementioned inferences, the confocal fluorescence imaging technique was applied to investigate the spatial distribution of fluorescent species, which has contributed to the direct observation of coke's location on large crystals [15,36,37]. Weckhuysen and co-workers investigated the absorption and fluorescence properties of coke species in H-ZSM-5 and H-SAPO-34 and then used fluorescence microscopy to monitor the in situ formation of coke during the MTO process [15,36]. It has been revealed that coke species in SAPO-34 crystals could exhibit fluorescence at λ = 510–550 and 565–635 nm in the visible-light region using different laser lights (λ = 488 and 561 nm) [15,36]. The UV–vis spectra of spent catalysts reveal a pronounced band at 400 nm, which is ascribed to the charged highly methylated benzene species at this moment (Fig. S5) [15]. Two broad absorbance peaks around 470 and 630 nm appeared at prolonged reaction time, which can be ascribed to bulky aromatics, such as charged methylated naphthalene species and polyaromatics [19,49,50]. The UV–vis absorption band at higher wavelengths can be rationalized by the formation of bulky organic species [15,36,50]. These organics are also detected in GC–MS chromatograms.

In the present work, since fresh catalyst did not fluoresce with excitation by 700 nm light in the analysis of fluorescence microphotographs, the background fluorescence signal from the SAPO-34 crystal could be excluded (Fig. 5b). The coke species within SAPO-34 also exhibited near-infrared (NIR) fluorescence (λ = 760–840 nm), which was then applied as a signal to study the bulky coke formation (Fig. 5). Therefore, fluorescence emissions were collected in the range 760–840 nm, which was excited by 700 nm light to detect polycyclic aromatic hydrocarbons. As shown in Fig. 5a, with the proceeding of the reaction and coke deposition, the crystals changed from colorless to yellow and became dark yellow after 49 min on stream in bright field images. Fig. 5b shows the fluorescence images of SAPO-34 crystals as a function of time on stream, in which the bright region represents the presence of fluorescent species. For the catalyst after reaction for 5 min, few fluorescent species were detected. When the reaction time was prolonged, the fluorescence presented at the edges and the diagonal of the crystal, as shown in Fig. 5b. The occurrence of fluorescence at the margin of the crystal originates from the contact and conversion of the reactant. The obvious crosslike feature fluorescence in the core of the crystal is mainly attributed to the heterogeneity of the internal structure of the crystal [51]. The complex intergrowth structure of the crystal may strongly affect the intracrystalline mass transport and cause preferential reaction and coke deposition at the interfaces of subunits with crosslike feature fluorescence; therefore, the cavities in the pyramid-shaped region of SAPO-34 crystals are less accessible for reactants [52,53]. After reaction for 18 min, a broadened fluorescent region was observed in the edges and cores of crystals. Based on the GC–MS and ^{129}Xe NMR analysis of the deactivated catalysts, it is reasonable to assume that the larger conjugated aromatic species, which deactivate SAPO-34 catalysts, are responsible for the observed fluorescence on the crystals.

This nonuniform spatial distribution of fluorescent coke species in the individual crystal correlates closely with the variation of the intracrystalline mass transport properties during the catalytic reaction. During the early reaction period, a small amount of coke precursor readily formed at the outer layer of the crystal and caused less intracrystalline diffusion limitation for reactants. Meanwhile, the spatial distribution of these fluorescent organic species presented crosslike pattern in the center of crystal along the interfaces of subunits. With the progress of methanol conversion, reactants moved forward into the core of the crystal and heavier coke compounds formed within the cavities due to secondary reaction. Thus, fluorescent region gradually expanded into square-shaped in the core of crystal. Simultaneously, fluorescent species located at the outer layer of the crystal became more dominant, arising from the accumulation of the majority of bulky coke species. Finally, the coke accumulation and complete pore blockage at the outer layer of the crystal prevented methanol from diffusing into the interior of the crystal, resulting in rapid catalyst deactivation with a yolk–shell-like spatial distribution of coke. This is also consistent with the results of HP ^{129}Xe NMR spectroscopy or nitrogen adsorption–desorption measurement, in which xenon or N_2 adsorption decreased obviously at 49 min. SAPO-34 catalyst deactivation by cutting off the reactant at the outer layer of the crystal also was observed in previous studies of the MTO process [15,36]. On the other hand, it has been reported that a nonuniform distribution of Si exists in SAPO molecular sieves and Si content increases from the core to the surface of crystals, resulting in higher acid density or strength at the outer layers of the crystals [54,55]. According to the results of XPS and XRF (Table S1), the Si content

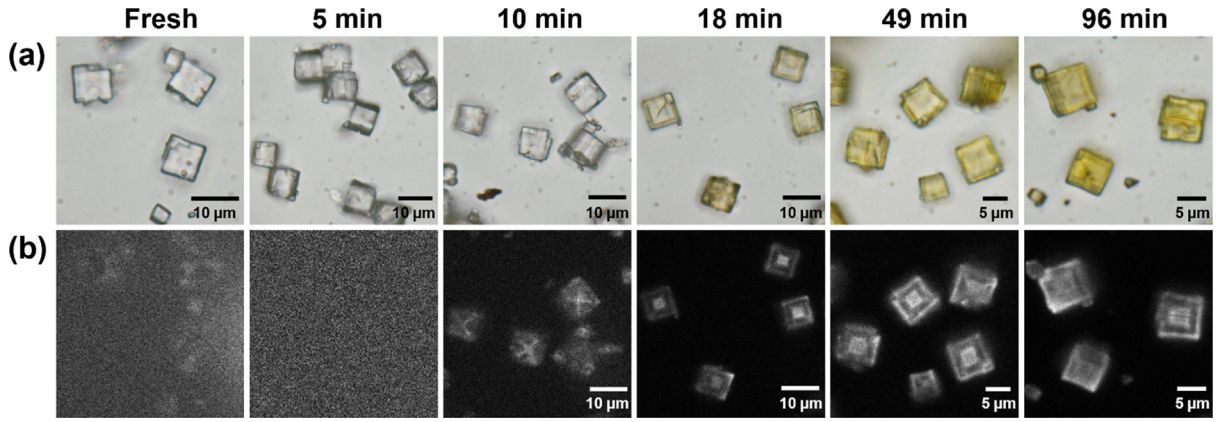

Fig. 5. Bright field images (a) and confocal fluorescence microscopy images (b) of SAPO-34 crystals after MTO conversion at 673 K for various reaction times. Fluorescence from the interior of the crystal.

of the external surface, determined by XPS, is higher than that in the bulk, determined by XRF. Therefore, the Si enrichment phenomenon is also observed on the surfaces of SAPO-34 crystals used in this work, which indicates that Brønsted acid sites are enriched on the external surfaces of crystals. Thus, the preferential location of coke species on the external surface also probably benefits from Si enrichment on the surfaces of crystals. On the basis of this analysis, it can be concluded that the heterogeneity of Brønsted acidity and the intracrystalline mass transport limitation eventually lead to a nonuniform spatial distribution of coke species within SAPO-34 catalyst. The formation and location of bulky organic species have a strong impact on the reaction via the indirect pathway mediated by the trapped organics and also strongly influence the mass transfer of reactants and products in the catalyst, which are of great significance for the proceeding of MTO [5,12,56].

3.3. The effect of coke species trapped inside SAPO-34 catalysts on acidic properties and mass transport

3.3.1. Acidic properties

Coke species located in the SAPO-34 catalyst, especially in the shell layers of the crystals, may reduce the accessibility of inner acidic sites due to strong intracrystalline diffusion limitations. In the present work, DRIFTS was used for the quantitative detection of unoccupied acidic sites of coked catalysts. The DRIFT spectra of all the spent catalysts after methanol conversion over SAPO-34 at 673 K present the stretching variation of the absorbance of hydroxyl groups and retained organics (Fig. S6). Two bands at around 3618 and 3596 cm^{-1} are assigned to two distinct families of bridging hydroxyl groups (Brønsted acid sites) [57,58]. The IR bands at 1564, 1510, and 1460 cm^{-1} are ascribed to the stretching vibrations of the C—C bonds of aromatics. The bands at 2956, 2930, and 2872 cm^{-1} represent the stretching vibration of the C—H bond, which show the formation of alkyl groups on aromatics [59,60]. Clearly, the bands related to aromatics showed enhanced intensity with reaction time. Due to interactions between hydroxyl groups and organics trapped within cavities, a sustained formation and accumulation of coke species caused the coverage of acidic sites and resulted in a pronounced reduction in the relative intensity of Brønsted acid sites with absorbance at both 3618 and 3596 cm^{-1} in the stage of 0–49 min (Fig. 6). More than 65% of bridge hydroxyl groups were still detected over the catalyst after reaction for 96 min. Combined with the result of nonuniform distribution of coke formed on crystals, this result could be explained by the fact that the growth of coke species toward larger polyaromatics became significant at the outer layer of the catalyst and the

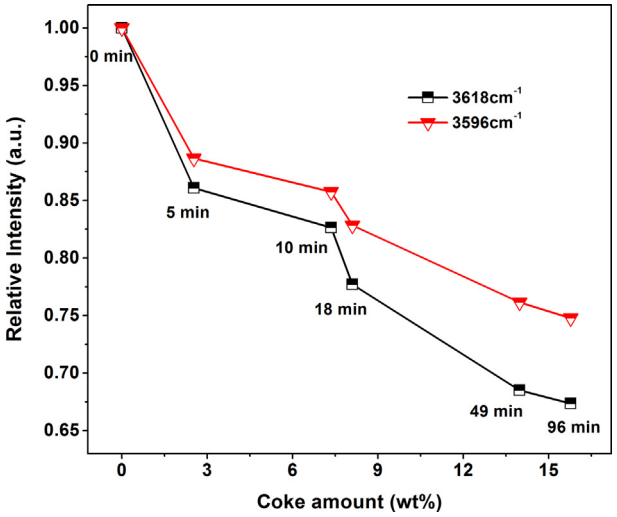

Fig. 6. The changes in relative intensity of Brønsted acid sites in spent catalysts with coke amount. The intensity of the bands of fresh SAPO-34 catalyst at 3618 and 3596 cm^{-1} was set as 1.00.

acidic sites located in the centers of crystals were difficult for the reactants to contact due to strong diffusion limitation. Hence, this result also implies that the catalyst deactivation mainly derives from the blockage of mass transfer paths at the shell layers of SAPO-34 crystals.

To verify this view, the fully deactivated SAPO-34 catalyst after reaction for 96 min was ground into smaller crystal particles in a mortar to expose the internal acidic sites in the catalyst. XRD patterns and SEM images of unbroken catalyst (sample A) and broken catalyst (sample B) are shown in Figs. S7 and S8, respectively. The ground sample still maintained the CHA topological structure, although the grain size of the sample was reduced. A comparative study of the MTO reaction was performed to evaluate the catalytic performance of fresh, unbroken, and broken catalysts under the same reaction conditions. As shown in Fig. S9, among the three catalysts, methanol can be completely converted over fresh SAPO-34, while methanol conversion over sample A (deactivated and unbroken catalyst) was only 11.7%. A relatively high methanol conversion (87%) was exhibited in the methanol reaction over sample B, the deactivated and broken SAPO-34 catalyst. These results confirmed that in the interior of the deactivated SAPO-34 catalyst, a large number of acidic sites were inaccessible for the reaction of methanol. The bulky coke species located at the outer layer of

the crystal led to a stronger limitation of reactant diffusion into the internal cavities of the catalyst. This finding of the accessible cavity reduction with coke formation is in agreement with the observations by HP ^{129}Xe NMR and confocal fluorescence spectroscopy.

3.3.2. The diffusion performance of the SAPO-34 catalyst during the methanol-to-olefins reaction

Detailed studies of the formation and distribution of coke as well as of acidic properties have shown that bulky coke species formation in the cavities of SAPO-34 reduced molecular mobility in the catalyst during the MTO reaction. Hence, in this section, a powerful technique, ^{1}H PFG NMR spectroscopy, was employed to evaluate the quantitative variation of mass transport in SAPO-34 with coke deposition from the microscopic perspective, using methane and ethene as probe molecules. A 7–10 μm SAPO-34 crystal (Fig. S2) was used in the PFG NMR experiment in the present study. The square roots of the mean squared displacement for methane and ethene are smaller than the crystal size, using a diffusion time of 15–20 ms and PFG NMR diffusion coefficients in the order of 10^{-11} and 10^{-12} m^2/s for methane and ethene, respectively, based on the Einstein equation [61],

$$6Dt = \langle r^2 \rangle, \quad (2)$$

where D is the self-diffusion coefficient, t is the diffusion time, and $\langle r^2 \rangle$ is the mean squared displacement.

Fig. S10 shows the decay of spin–echo attenuation of ^{1}H PFG NMR for methane and ethene in SAPO-34 catalyst recorded at 298 K with increasing the gradient strength. Self-diffusion coefficients were determined by fitting the PFG NMR data with Eq. (1). Initially, at the reaction stage of 0–18 min, in which the catalyst possessed high reactivity with complete methanol conversion, a decrease of the diffusion coefficient was exhibited for methane in the SAPO-34 catalyst with a loading of 0.5 molecules per cage at 298 K, as shown in Fig. 7a. During this period, the formation of methylbenzenes and methylnaphthalenes in the catalyst gave rise to a decline of the diffusion coefficient, from 4.11×10^{-11} m^2/s for fresh catalyst to 3.53×10^{-11} m^2/s at a TOS of 10 min and further to 2.71×10^{-11} m^2/s at a TOS of 18 min. When the reaction was prolonged to 49 min, the diffusion coefficient of methane declined to 3.08×10^{-12} m^2/s in the deactivated catalyst with a coke amount of 13.9 wt%. When the reaction time was further prolonged, the diffusion coefficient of methane was found to decrease slowly to 1.92×10^{-12} m^2/s at 96 min. This trend in methane diffusivity could be attributed to pore modification and cavity occupation by the formation and accumulation of aromatic species inside SAPO-34. A very low self-diffusion coefficient at 49 min could be ascribed to severe pore modification with bulky coke species; comparatively, the reduction in diffusivity during the stage of 49–96 min was less remarkable with the slowdown of coke deposition. A similar evolution was also seen for detectable micropore volume and BET surface area of the catalyst in nitrogen adsorption–desorption measurements. Cavity occupation and channel blockage by coke species directly lead to mass transport reduction. Similarly, ethene, as one of the most important products, was also used to probe the diffusivity in the MTO reaction. The intracrystalline diffusion coefficient of ethene, with a larger diameter than that of methane, showed lower diffusivity than that of methane in the coked catalyst at a loading of 0.5 molecules per CHA cage (Fig. 7a). Especially, it is found that ethene exhibited a sharper reduction in the diffusion coefficient than methane from 0 to 5 min on stream. The lower ethene diffusivity could also be rationalized by its greater molecular size, and the SAPO-34 catalyst with eight-membered ring windows and cavity structure imposes a stronger diffusion limitation effect on ethene than on methane in a confined environment. The self-diffusion coefficient of ethene decreased significantly after reaction for 18 min and the diffusion was too slow to measure reliably at reaction times of 49 and 96 min. During this procedure, stronger diffusion limitation also occurred for hydrocarbon products generation, corresponding to the gradual variation of the product distribution and the deactivation of the catalyst.

The apparent intracrystalline diffusion activation energies (E_a) of adsorbate (CH_4 and C_2H_4) (Fig. 7b) in the fresh and spent catalysts were calculated on the basis of the Arrhenius law:

$$D = D_0 \exp(-E_a/RT). \quad (3)$$

The Arrhenius plots of adsorbed molecules recorded in the temperature range 298–328 K are presented in Fig. S11. As indicated in Fig. 7b, the apparent intracrystalline diffusion activation energies of methane in spent catalysts increased slightly from reaction times of 5–18 min, and attained a high value at 49 min on stream, representing strong intracrystalline diffusion limitation with coke formation in the catalyst and corresponding well to the variation of the diffusion coefficient of methane. The apparent diffusion activation energies of ethene with TOS also increased with coke formation on the catalyst. Therefore, coke formation and deposition are the main cause for intracrystalline diffusion limitation by modifying pores or cavities during the MTO reaction over SAPO-34. In a heavily deactivated catalyst, pore blockage and cavity occupation become significant and mass transport of reactants and products is strongly restricted.

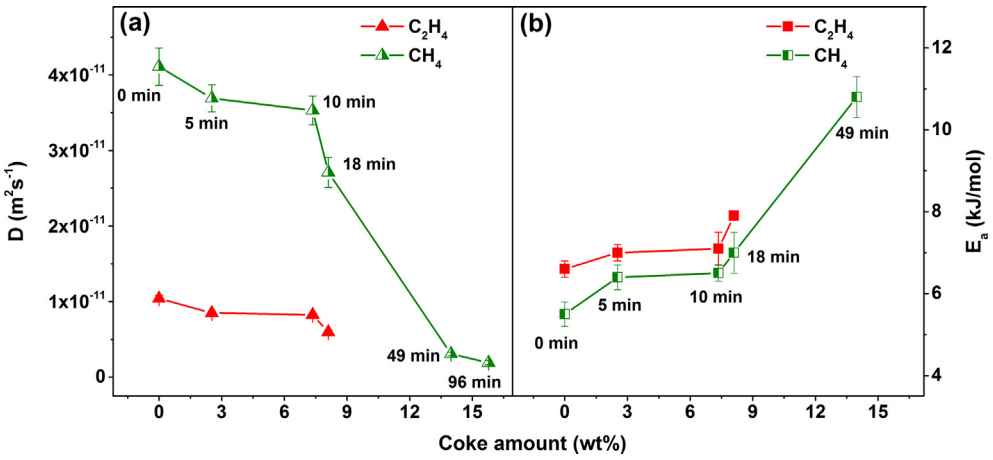

Fig. 7. The variation in intracrystalline self-diffusion coefficients of CH_4 and C_2H_4 at 298 K (a) and diffusion activation energies determined in the temperature range 298–328 K (b) in fresh and spent SAPO-34 as a function of coke amount. A loading of 0.5 molecules per cage is used.

4. Conclusions

In the present work, the complete course of methanol reaction and deactivation over SAPO-34 with a crystal size of 7–10 μm has been studied. The nature and the spatial location of confined coke species and the variation of mass transport and accessible active sites with coke deposition in SAPO-34 catalysts shed more light on the complicated deactivation mode of methanol conversion over cavity-type and eight-membered-ring SAPO catalysts.

The evolution of confined organics in SAPO-34 during methanol conversion, from methylbenzenes and methylnaphthalenes at the beginning of the reaction to polyaromatics such as phenanthrene and pyrene during deactivation, corresponds to the process of MTO reaction and deactivation. The decrease in micropore volume probed by nitrogen adsorption–-desorption or xenon adsorption measured by HP ^{129}Xe NMR results from the occupation of CHA cavities by coke species. A nonuniform spatial distribution of the fluorescent organic species in SAPO-34 crystals was presented by CFM with a yolk–shell-like feature. The occupation of the cavities in the shell layers of the crystals causes a great reduction in mass transport of reactant and products, characteristic of the decreased self-diffusion coefficient and the increased diffusion activation energy, which are evaluated by PFG NMR measurement using methane and ethene as probe molecules. With the formation and accumulation of bulky coke species in the shell layers of the crystals, the acidic sites in the inner parts of the catalyst crystals would be shielded and become inaccessible for the reactant methanol. The evolution of initially formed confined organics to coke species, the nonuniform coke formation in SAPO-34 crystals, and the reduced molecular diffusion behavior and accessible acidic sites caused by the spatial heterogeneity of coke formation in the SAPO-34-catalyzed MTO reaction all lead to the deactivation of the MTO reaction in cavity-type SAPO catalysts with narrow pore openings.

Acknowledgments

The authors thank the National Natural Science Foundation of China (Nos. 21473182, 91545104, 91745109, 21422606), the Youth Innovation Promotion Association of the Chinese Academy of Sciences (2014165), and the Key Research Program of Frontier Sciences, Chinese Academy of Sciences (Grant QYZDY-SSW-JSC024) for financial support. Z.C. Xu thanks DICP DMTO201603 for financial support. The authors declare no competing financial interest.

Appendix A. Supplementary material

Supplementary data to this article can be found online at https://doi.org/10.1016/j.jcat.2018.09.010.

References

[1] M. Stöcker, Micropor. Mesopor. Mater. 29 (1999) 3–48.
[2] U. Olsbye, S. Svelle, M. Bjørgen, P. Beato, T.V.W. Janssens, F. Joensen, S. Bordiga, K.P. Lillerud, Angew. Chem. Int. Ed. 51 (2012) 5810–5831.
[3] P. Tian, Y.X. Wei, M. Ye, Z.M. Liu, ACS Catal. 5 (2015) 1922–1938.
[4] Y. Bhawe, M. Moliner-Marin, J.D. Lunn, Y. Liu, A. Malek, M. Davis, ACS Catal. 2 (2012) 2490–2495.
[5] J.Z. Li, Y.X. Wei, J.R. Chen, S.T. Xu, P. Tian, X.F. Yang, B. Li, J.B. Wang, Z.M. Liu, ACS Catal. 5 (2015) 661–665.
[6] S. Teketel, L.F. Lundegaard, W. Skistad, S.M. Chavan, U. Olsbye, K.P. Lillerud, P. Beato, S. Svelle, J. Catal. 327 (2015) 22–32.
[7] M. Dyballa, P. Becker, D. Trefz, E. Klemm, A. Fischer, H. Jakob, M. Hunger, Appl. Catal. A Gen. 510 (2016) 233–243.
[8] I.M. Dahl, S. Kolboe, J. Catal. 149 (1994) 458–464.
[9] I.M. Dahl, S. Kolboe, J. Catal. 161 (1996) 304–309.
[10] W.G. Song, J.F. Haw, J.B. Nicholas, C.S. Heneghan, J. Am. Chem. Soc. 122 (2000) 10726–10727.
[11] B. Arstad, S. Kolboe, J. Am. Chem. Soc. 123 (2001) 8137–8138.
[12] J.F. Haw, W.G. Song, D.M. Marcus, J.B. Nicholas, Acc. Chem. Res. 36 (2003) 317–326.
[13] M. Guisnet, P. Magnoux, Appl. Catal. A Gen. 212 (2001) 83–96.
[14] S. Ilias, A. Bhan, ACS Catal. 3 (2013) 18–31.
[15] D. Mores, E. Stavitski, M.H.F. Kox, J. Kornatowski, U. Olsbye, B.M. Weckhuysen, Chem. Eur. J. 14 (2008) 11320–11327.
[16] W.L. Dai, M. Scheibe, L.D. Li, N.J. Guan, M. Hunger, J. Phys. Chem. C 116 (2012) 2469–2476.
[17] Y.X. Wei, J.Z. Li, C.Y. Yuan, S.T. Xu, Y. Zhou, J.R. Chen, Q.Y. Wang, Q. Zhang, Z.M. Liu, Chem. Commun. 48 (2012) 3082–3084.
[18] Y.X. Wei, C.Y. Yuan, J.Z. Li, S.T. Xu, Y. Zhou, J.R. Chen, Q.Y. Wang, L. Xu, Y. Qi, Q. Zhang, Z.M. Liu, ChemSusChem 5 (2012) 906–912.
[19] J. Goetze, F. Meirer, I. Yarulina, J. Gascon, F. Kapteijn, J. Ruiz-Martínez, B.M. Weckhuysen, ACS Catal. 7 (2017) 4033–4046.
[20] D. Rojo-Gama, M. Signorile, F. Bonino, S. Bordiga, U. Olsbye, K.P. Lillerud, P. Beato, S. Svelle, J. Catal. 351 (2017) 33–48.
[21] D.S. Wragg, M.G. O'Brien, F.L. Bleken, M. Di Michiel, U. Olsbye, H. Fjellvåg, Angew. Chem. Int. Ed. 51 (2012) 7956–7959.
[22] W.G. Song, H. Fu, J.F. Haw, J. Phys. Chem. B 105 (2001) 12839–12843.
[23] K. Hemelsoet, A. Nollet, M. Vandichel, D. Lesthaeghe, V. Van Speybroeck, M. Waroquier, ChemCatChem 1 (2009) 373–378.
[24] D. Chen, K. Moljord, T. Fuglerud, A. Holmen, Micropor. Mesopor. Mater. 29 (1999) 191–203.
[25] W.L. Dai, G.J. Wu, L.D. Li, N.J. Guan, M. Hunger, ACS Catal. 3 (2013) 588–596.
[26] K.Y. Lee, H.-J. Chae, S.-Y. Jeong, G. Seo, Appl. Catal. A Gen. 369 (2009) 60–66.
[27] B.P.C. Hereijgers, F. Bleken, M.H. Nilsen, S. Svelle, K.-P. Lillerud, M. Bjørgen, B. M. Weckhuysen, U. Olsbye, J. Catal. 264 (2009) 77–87.
[28] G.J. Yang, Y.X. Wei, S.T. Xu, J.R. Chen, J.Z. Li, Z.M. Liu, J.H. Yu, R.R. Xu, J. Phys. Chem. C 117 (2013) 8214–8222.
[29] N. Nishiyama, M. Kawaguchi, Y. Hirota, D. Van Vu, Y. Egashira, K. Ueyama, Appl. Catal. A Gen. 362 (2009) 193–199.
[30] A.M. Zheng, S.H. Li, S.B. Liu, F. Deng, Acc. Chem. Res. 49 (2016) 655–663.
[31] A.M. Zheng, S.B. Liu, F. Deng, Chem. Rev. 117 (2017) 12475–12531.
[32] T.Y. Liang, J.L. Chen, Z.F. Qin, J.F. Li, P.F. Wang, S. Wang, G.F. Wang, M. Dong, W. B. Fan, J.G. Wang, ACS Catal. 6 (2016) 7311–7325.
[33] M. Guisnet, L. Costa, F.R. Ribeiro, J. Mol. Catal. A Chem. 305 (2009) 69–83.
[34] F. Bleken, M. Bjørgen, L. Palumbo, S. Bordiga, S. Svelle, K.-P. Lillerud, U. Olsbye, Top. Catal. 52 (2009) 218–228.
[35] W.L. Dai, G. Cao, L. Yang, G.J. Wu, M. Dyballa, M. Hunger, N.J. Guan, L.D. Li, Catal. Sci. Technol. 7 (2017) 607–618.
[36] Q.Y. Qian, J. Ruiz-Martinez, M. Mokhtar, A.M. Asiri, S.A. Al-Thabaiti, S.N. Basahel, H.E. van der Bij, J. Kornatowski, B.M. Weckhuysen, Chem. Eur. J. 19 (2013) 11204–11215.
[37] Q.Y. Qian, J. Ruiz-Martínez, M. Mokhtar, A.M. Asiri, S.A. Al-Thabaiti, S.N. Basahel, B.M. Weckhuysen, Catal. Today 226 (2014) 14–24.
[38] Y. Liu, W.P. Zhang, S.J. Xie, L.Y. Xu, X.W. Han, X.H. Bao, J. Phys. Chem. B 112 (2008) 1226–1231.
[39] F. Guenneau, K. Panesar, A. Nossov, M.-A. Springuel-Huet, T. Azais, F. Babonneau, C. Tourne-Peteilh, J.-M. Devoisselle, A. Gedeon, Phys. Chem. Chem. Phys. 15 (2013) 18805–18808.
[40] S.T. Xu, W.P. Zhang, X.C. Liu, X.W. Han, X.H. Bao, J. Am. Chem. Soc. 131 (2009) 13722–13727.
[41] A. Nossov, F. Guenneau, M.-A. Springuel-Huet, E. Haddad, V. Montouillout, B. Knott, F. Engelke, C. Fernandez, A. Gedeon, Phys. Chem. Chem. Phys. 5 (2003) 4479–4483.
[42] J. Kärger, ChemPhysChem 16 (2015) 24–51.
[43] C. Chmelik, D. Freude, H. Bux, J. Haase, Micropor. Mesopor. Mater. 147 (2012) 135–141.
[44] A. Galarneau, F. Guenneau, A. Gedeon, D. Mereib, J. Rodriguez, F. Fajula, B. Coasne, J. Phys. Chem. C 120 (2016) 1562–1569.
[45] S.M. Csicsery, Zeolites 4 (1984) 202–213.
[46] J. Kärger, R. Valiullin, Chem. Soc. Rev. 42 (2013) 4172–4197.
[47] R.M. Cotts, M.J.R. Hoch, T. Sun, J.T. Markert, J. Magn. Reson. (1969–1992) 83 (1989,) 252–266.
[48] J.L. Bonardet, M.C. Barrage, J. Fraissard, J. Mol. Catal. A Chem. 96 (1995) 123–143.
[49] K. De Wispelaere, C.S. Wondergem, B. Ensing, K. Hemelsoet, E.J. Meijer, B.M. Weckhuysen, V. Van Speybroeck, J. Ruiz-Martínez, ACS Catal. 6 (2016) 1991–2002.
[50] D. Mores, J. Kornatowski, U. Olsbye, B.M. Weckhuysen, Chem. Eur. J. 17 (2011) 2874–2884.
[51] L. Karwacki, E. Stavitski, M.H.F. Kox, J. Kornatowski, B.M. Weckhuysen, Angew. Chem. Int. Ed. 46 (2007) 7228–7231.
[52] E. Lehmann, C. Chmelik, H. Scheidt, S. Vasenkov, B. Staudte, J. Kärger, F. Kremer, G. Zadrozna, J. Kornatowski, J. Am. Chem. Soc. 124 (2002) 8690–8692.
[53] G. Muller, T. Narbeshuber, G. Mirth, J.A. Lercher, J. Phys. Chem. 98 (1994) 7436–7439.
[54] P. Tian, B. Li, S.T. Xu, X. Su, D.H. Wang, L. Zhang, D. Fan, Y. Qi, Z.M. Liu, J. Phys. Chem. C 117 (2013) 4048–4056.
[55] G.Y. Liu, P. Tian, Y. Zhang, J.Z. Li, L. Xu, S.H. Meng, Z.M. Liu, Micropor. Mesopor. Mater. 114 (2008) 416–423.
[56] I. Pinilla-Herrero, U. Olsbye, C. Marquez-Alvarez, E. Sastre, J. Catal. 352 (2017) 191–207.
[57] S. Bordiga, L. Regli, D. Cocina, C. Lamberti, M. Bjørgen, K.P. Lillerud, J. Phys. Chem. B 109 (2005) 2779–2784.

[58] L. Smith, A.K. Cheetham, L. Marchese, J.M. Thomas, P.A. Wright, J. Chen, E. Gianotti, Catal. Lett. 41 (1996) 13–16.
[59] J.W. Park, G. Seo, Appl. Catal. A Gen. 356 (2009) 180–188.
[60] L.M. Petkovic, D.M. Ginosar, K.C. Burch, J. Catal. 234 (2005) 328–339.
[61] A. Einstein, Investigations on the Theory of the Brownian Movement, Dover, New York, 1956.